Bat and Rat Neurons Differ in Theta-Frequency Resonance Despite Similar Coding of Space

James G. Heys *et al.*

Science **340**, 363 (2013);
DOI: 10.1126/science.1233831

Science (print ISSN 0036-8075; online ISSN 1095-9203) is published weekly, except the last week in December, by the American Association for the Advancement of Science, 1200 New York Avenue NW, Washington, DC 20005.

These fingerlike protrusions contained Eff-1 clusters on the membrane (Fig. 4F, d and d′′) and were anchored at their basal side by exogenous αPS2 (Fig. 4, F and G, d to d′′). As in Sns-Eff-1–expressing cells (Fig. 3A′′), the invasive fingers in αPS2-Eff-1–expressing cells contained segments of electron-dense ladders (Fig. 3B′′) corresponding to the Eff-1 clusters observed by STORM (Fig. 4F, d′ and d′′). Thus, despite the differences in the requirement of actin regulators (Scar versus Scar-WASP) and the overall morphology of F-actin enrichment (hairs versus foci), αPS2-Eff-1–expressing cells and Sns-Eff-1–expressing cells use similar invasive fingerlike membrane protrusions to promote fusogenic protein engagement during cell fusion.

Our studies reveal two fundamental principles underlying cell-cell fusion. First, a transmembrane fusogenic protein is indispensable for cell-cell fusion, because fusion does not occur without a fusogenic protein, irrespective of actin cytoskeletal remodeling. Second, the actin cytoskeleton provides an active driving force for cell-cell fusion by generating membrane protrusions that are necessary and sufficient to promote fusion mediated by fusogenic proteins. Membrane protrusions induced by different adhesion molecules share common characteristics of invasiveness and engagement of fusogenic proteins and therefore represent a general cell-cell fusion mechanism.

References and Notes

1. E. H. Chen, E. N. Olson, *Science* **308**, 369 (2005).
2. B. M. Ogle, M. Cascalho, J. L. Platt, *Nat. Rev. Mol. Cell Biol.* **6**, 567 (2005).
3. M. Oren-Suissa, B. Podbilewicz, *Trends Cell Biol.* **17**, 537 (2007).
4. O. Avinoam, B. Podbilewicz, *Curr. Top. Membr.* **68**, 209 (2011).
5. K. Rochlin, S. Yu, S. Roy, M. K. Baylies, *Dev. Biol.* **341**, 66 (2010).
6. E. H. Chen, *Curr. Top. Membr.* **68**, 235 (2011).
7. S. M. Abmayr, G. K. Pavlath, *Development* **139**, 641 (2012).
8. S. Yanagawa, J. S. Lee, A. Ishimoto, *J. Biol. Chem.* **273**, 32353 (1998).
9. M. Ruiz-Gómez, N. Coutts, A. Price, M. V. Taylor, M. Bate, *Cell* **102**, 189 (2000).
10. B. A. Bour, M. Chakravarti, J. M. West, S. M. Abmayr, *Genes Dev.* **14**, 1498 (2000).
11. S. Kim *et al.*, *Dev. Cell* **12**, 571 (2007).
12. R. Massarwa, S. Carmon, B. Z. Shilo, E. D. Schejter, *Dev. Cell* **12**, 557 (2007).
13. G. Schäfer *et al.*, *Dev. Biol.* **304**, 664 (2007).
14. B. E. Richardson, K. Beckett, S. J. Nowak, M. K. Baylies, *Development* **134**, 4357 (2007).
15. W. A. Mohler *et al.*, *Dev. Cell* **2**, 355 (2002).
16. B. Podbilewicz *et al.*, *Dev. Cell* **11**, 471 (2006).
17. H. A. Dworak, M. A. Charles, L. B. Pellerano, H. Sink, *Development* **128**, 4265 (2001).
18. B. J. Galletta, M. Chakravarti, R. Banerjee, S. M. Abmayr, *Mech. Dev.* **121**, 1455 (2004).
19. E. H. Chen, B. A. Pryce, J. A. Tzeng, G. A. Gonzalez, E. N. Olson, *Cell* **114**, 751 (2003).
20. R. Islam, S. Y. Wei, W. H. Chiu, M. Hortsch, J. C. Hsu, *Development* **130**, 2051 (2003).
21. C. A. Johnston, K. Hirono, K. E. Prehoda, C. Q. Doe, *Cell* **138**, 1150 (2009).
22. P. J. Gotwals, S. E. Paine-Saunders, K. A. Stark, R. O. Hynes, *Curr. Opin. Cell Biol.* **6**, 734 (1994).
23. M. Schwander *et al.*, *Dev. Cell* **4**, 673 (2003).
24. P. Fénichel, M. Durand-Clément, *Hum. Reprod.* **13** (suppl. 4), 31 (1998).
25. A. K. McNally, J. M. Anderson, *Am. J. Pathol.* **160**, 621 (2002).
26. N. Tabata *et al.*, *J. Immunol.* **153**, 3256 (1994).
27. K. L. Sens *et al.*, *J. Cell Biol.* **191**, 1013 (2010).
28. S. Haralalka *et al.*, *Development* **138**, 1551 (2011).
29. K. A. Edwards, M. Demsky, R. A. Montague, N. Weymouth, D. P. Kiehart, *Dev. Biol.* **191**, 103 (1997).
30. M. J. Rust, M. Bates, X. Zhuang, *Nat. Methods* **3**, 793 (2006).
31. P. Jin *et al.*, *Dev. Cell* **20**, 623 (2011).
32. R. Duan *et al.*, *J. Cell Biol.* **199**, 169 (2012).
33. O. Avinoam *et al.*, *Science* **332**, 589 (2011).

Acknowledgments: We thank P. Beachy for the S2R+ cell line and G. Seydoux for the *C. elegans* cDNA; M. Delannoy at Johns Hopkins Microscope Facility for advice on cell culture TEM and immunoEM; J. Reidler, J. Hill, and J. DeWitt at Nikon Instruments Inc. for advice on STORM; and S. Craig, J. Nathans, E. Olson, D. Pan, D. Robinson, G. Seydoux, J. Yang, and members of the Chen lab for discussions and critical reading of the manuscript. K.S. was a postdoctoral fellow of the American Heart Association. Supported by the National Institutes of Health (R01 GM098816) and the Packard Foundation (E.H.C.).

Supplementary Materials

www.sciencemag.org/cgi/content/full/science.1234781/DC1
Materials and Methods
Figs. S1 to S14
Table S1
Movies S1 to S10
References (*34*–*36*)

4 January 2013; accepted 22 February 2013
Published online 7 March 2013;
10.1126/science.1234781

Bat and Rat Neurons Differ in Theta-Frequency Resonance Despite Similar Coding of Space

James G. Heys,[1]* Katrina M. MacLeod,[2] Cynthia F. Moss,[3] Michael E. Hasselmo[4]*

Both bats and rats exhibit grid cells in medial entorhinal cortex that fire as they visit a regular array of spatial locations. In rats, grid-cell firing field properties correlate with theta-frequency rhythmicity of spiking and membrane-potential resonance; however, bat grid cells do not exhibit theta rhythmic spiking, generating controversy over the role of theta rhythm. To test whether this discrepancy reflects differences in rhythmicity at a cellular level, we performed whole-cell patch recordings from entorhinal neurons in both species to record theta-frequency resonance. Bat neurons showed no theta-frequency resonance, suggesting grid-cell coding via different mechanisms in bats and rats or lack of theta rhythmic contributions to grid-cell firing in either species.

The medial entorhinal cortex (mEC) of rodents, humans, nonhuman primates, and bats encodes space by using similar neural firing patterns (*1*–*5*). Unit recordings from awake-behaving rodents and bats demonstrate that single neurons in the mEC, termed grid cells, fire when an animal traverses spatial locations on a periodic triangular array, tiling the environment. In rodents, grid-cell coding correlates with rhythmicity at theta frequency (4 to 10 Hz). Subthreshold membrane-potential resonance (sMPR) at theta frequency matches the anatomical distribution of grid cells (*6*) and differs along the dorsal-to-ventral axis of rodent mEC (*7*–*11*), in proportion with grid-cell firing field properties (*2*). Rodent grid-cell spiking shows precession in theta phase relative to location (*12*), theta rhythmicity correlated with grid field properties and running velocity (*13*, *14*), and loss of spatial periodicity in the absence of network theta rhythm (*15*, *16*).

However, bat recordings demonstrate grid cells in mEC and place cells in the hippocampus in the absence of continuous theta-frequency rhythmicity in field potentials or spike-train autocorrelograms (*5*, *17*), arguing against theta-rhythmic mechanisms for grid-cell firing, but controversy remains that theta rhythmicity could be masked by low firing rates in bat grid cells (*18*). To test for intrinsic theta-rhythmic mechanisms in the bat species *Eptesicus fuscus* and *Rousettus aegyptiacus*, we made in vitro whole-cell patch recordings in brain slices, looking for theta-frequency sMPR. In contrast to layer II stellate cells in rodent mEC, layer II neurons of bat mEC do not show theta-frequency sMPR. These data corroborate earlier bat unit recording data (*5*, *17*) showing that continuous theta rhythmicity during navigation is not present in all mammalian species.

Previous studies demonstrated that parahippocampal areas in bat and rodent brains show similar anatomical organization (*5*, *19*, *20*). Neurons loaded with biocytin during whole-cell patch clamp recordings in horizontal brain slices were stained to reveal position and morphology (Fig. 1). Rat neurons were layer II stellate cells on the

[1]Graduate Program for Neuroscience, Center for Memory and Brain, Boston University, 2 Cummington Street, Boston, MA 02215, USA. [2]Department of Biology, University of Maryland, College Park, MD 20742, USA. [3]Department of Psychology, University of Maryland, College Park, MD 20742, USA. [4]Department of Psychology, Center for Memory and Brain, Boston University, 2 Cummington Street, Boston, MA 02215, USA.

*Corresponding author. E-mail: hasselmo@bu.edu (M.E.H.); jimheys@bu.edu (J.G.H.)

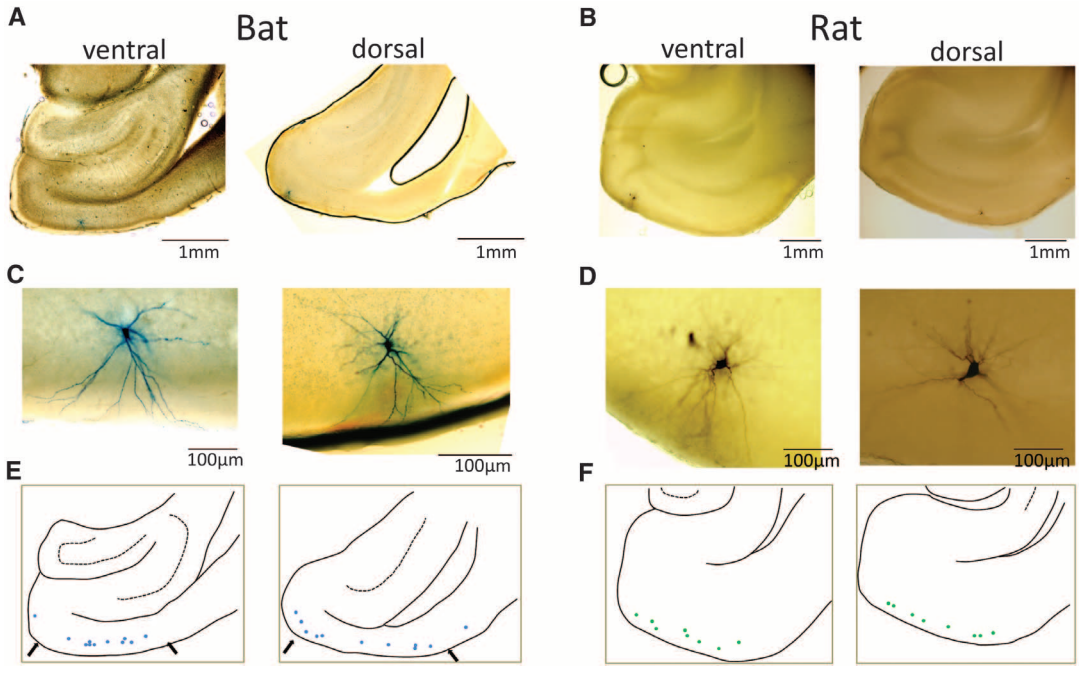

Fig. 1. Anatomy and morphology of layer II mEC neurons in bat and rat. Low-power images of neurons recorded in mECs from bat (**A**) and rat (**B**) in ventral (left) and dorsal (right) positions. High-power images show that mEC neurons in bat (**C**) and rat (**D**) have stellatelike appearance in ventral (left) and dorsal (right) locations. Recording locations labeled for bat (blue) (**E**) and rat neurons (green) (**F**) in ventral (left) and dorsal slices (right). Arrows indicate approximate mEC borders based on anatomical studies (*20*).

basis of position, morphology, and electrophysiology (*21*, *22*). Bat neurons showed similar patterns of arborization compared to rat stellate cells (Fig. 1, C and D). To ensure that bat recordings included mEC neurons, we sampled a wide range of medial to lateral parahippocampal positions (Fig. 1E and fig. S1).

Recordings from layer II mEC cells with stellate morphology demonstrate prominent electrophysiological differences between the species. Impedance profiles from bat layer II cells do not show the characteristic theta-frequency sMPR present in rat stellate cells (Fig. 2 and fig. S2). Mean resonance frequency measured at a membrane potential of –70 mV in bat neurons was 1.67 ± 0.13 Hz (SE) (n = 24), contrasting with theta-band resonance frequency in rat of 8.45 ± 1.19 Hz (n = 13) (P < 0.01) (Fig. 2E). Mean resonance frequency at –80 mV in bat was 1.77 ± 0.17 Hz (n = 24) and 8.86 ± 1.03 Hz (n = 12) in rat (P < 0.01) (Fig. 2F). Mean resonance strength in bat was 1.10 ± 0.02 at –70 mV (Fig. 2E) and 1.06 ± 0.01 (n = 24 cells) at –80 mV (Fig. 2F). In contrast, rat neurons show a band-pass impedance profile with a mean resonance strength of 1.47 ± 0.07 (n = 13) (P < 0.01) at –70 mV (Fig. 2E) and 1.36 ± 0.04 (n = 12 cells) (P < 0.01) at –80 mV (Fig. 2F).

Rat stellate cells show a large, inwardly rectifying current during hyperpolarizing input from expression of h current (I_h) (*22*–*24*), causing a depolarizing sag in voltage. Bat mEC neurons had significantly smaller sag ratio at multiple membrane potentials [sag ratio at –80 mV for bat was 0.13 ± 0.02 (n = 26 cells); for rat, 0.32 ± 0.02 (n = 14 cells) (P < 0.01)] (Fig. 3B). The sag time constant was significantly slower in bat neurons [sag time constant at –80 mV in bat, 178.88 ±

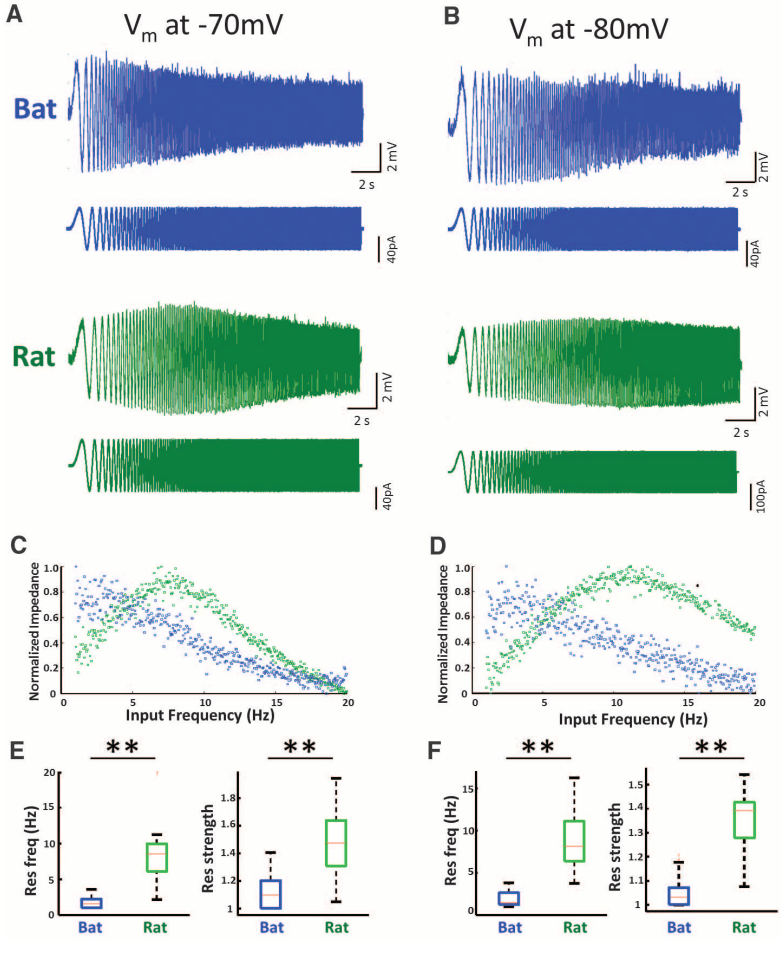

Fig. 2. Lack of theta-frequency resonance in bat neurons. Responses are shown for single bat neurons (blue, top) and single rat stellate cells (green, bottom), measured at membrane potentials (V_m) of –70 (**A**) and –80 mV (**B**). Normalized impedance plots from responses shown in (A) and (B) are depicted in (**C**) and (**D**). Box plots depict the quartiles of the resonance frequency measured at –70 (**E**) and –80 mV (**F**). **P < 0.01.

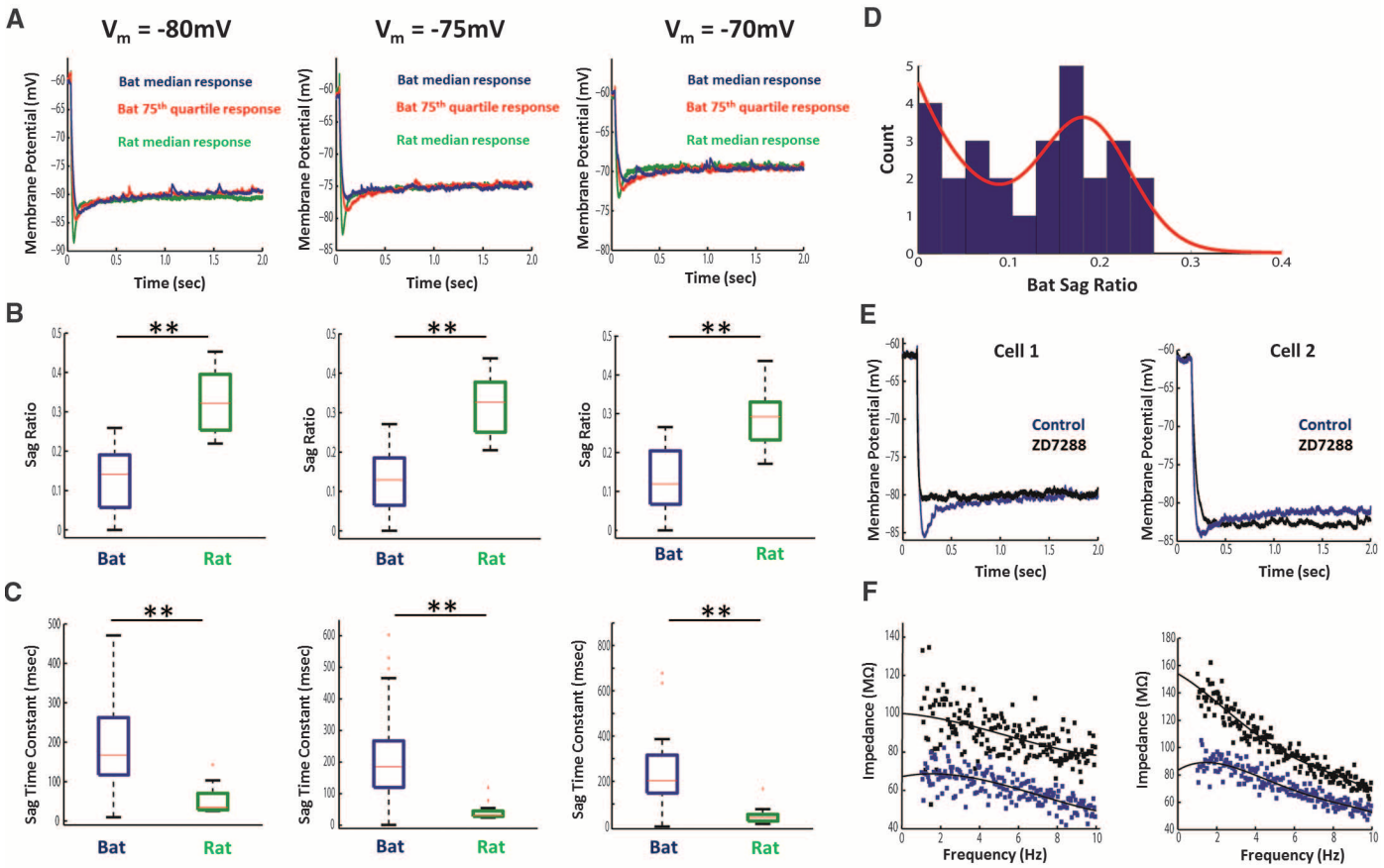

Fig. 3. Membrane potential sag is weaker and slower in bat neurons. (**A**) Voltage responses measured at steady-state membrane potentials of −80 (left), −75 (middle), and −70 mV (right). Sag ratios (**B**) and time constants (**C**) in bat (blue) and rat (green) neurons at −80 (left), −75 (middle), and −70 mV (right). $^{**}P < 0.01$. (**D**) A histogram of bat sag ratios at −80 mV appears bimodal. (**E**) Sag responses in bat cell 1 (left) and cell 2 (right) in control are abolished in 10 μM ZD788. (**F**) Impedance profile in control for cell 1 (left) and cell 2 (right) in control and after application of ZD7288.

24.55 ms (n = 24); in rat, 53.45 ± 9.85 ms (n = 14) ($P < 0.01$)] (Fig. 3C). However, inward rectification was still notable in many bat cells. The sag ratio across all bat neurons at –80 mV exhibited a bimodal distribution (Fig. 3D). With a third-order Gaussian fit, the second mode occurred at a sag ratio of 0.181. The 75th quartile sag response reflects the larger sag response in some bat neurons (Fig. 3A). The mean resonance frequency of bat neurons exhibiting the largest quartile sag ratio is still well below theta frequency (2.12 ± 0.32 Hz, n = 6). To demonstrate that sag in bat neurons arises from h current, we applied hyperpolarizing current steps in control artificial cerebrospinal fluid and after bath application of 10 μM ZD7288. Sag response (Fig. 3E) and resonance (Fig. 3F) were abolished after blockade of I_h (input current was adjusted for initial voltage of –60 mV and steady-state voltage of –80 mV), consistent with loss of theta frequency sMPR and sag in rat stellate cells during blockade of h current or genetic knockout of HCN1 (*8*, *10*, *24*, *25*).

Even bat neurons showing sag potentials did not reveal theta-frequency sMPR. To explain this, we built two biophysical conductance models (materials and methods) with morphological and electrophysiological properties of bat and rat neurons. A simplified model used h-current conductance density (G_h) and time constant (τ_h) based on single exponential fit to the sag response (Fig. 4A). The optimal parameterization combines lower-amplitude G_h (Fig. 4C, left) and slower τ_h (Fig. 4C, right) to match the sag response and non–theta-frequency resonance in bat experiments compared with theta-frequency resonance in rats (Fig. 4E). For rat and bat neurons, 20,000 simulations with different parameters showed that the experimentally derived sag ratio and time constant only occur at a single localized region of parameter space (Fig. 4G). By using a double exponential form of I_h, models simulated both the fast and slow component of the sag response (Fig. 4B). Similar to previous models of rat stellate cells (*10*, *23*, *26*), optimal fits gave a fast h current conductance density about 4.5 times larger than slow h current (Fig. 4D). In contrast, best fits for the bat gave a slow h current conductance density 1.3 times larger than the fast conductance (Fig. 4D).

The lack of theta rhythmicity in spike-train autocorrelograms from bat grid cells and place cells (*5*, *17*) has been argued to result from the low firing rate and short recording time of bat neurons that could obscure theta rhythmicity (*18*). To address these issues, our study sought to directly measure intrinsic intracellular mechanisms and showed a lack of theta-frequency properties in layer II neurons with stellate morphology in the bat, unlike the theta-frequency resonance of rat stellate cells. In line with other work (*5*), this suggests that theta-frequency resonance in the bat cannot provide a mechanism for grid-cell models (*27*). The lack of continuous theta-rhythmic spiking in the behaving bat and theta-rhythmic intrinsic cellular properties in slices of bat entorhinal cortex suggest that continuous theta may not be a general cross-species physiological mechanism in the mammalian entorhinal cortex and hippocampus (*5*, *17*). Bat neurons do show a peak in the impedance profile below 2 Hz, hinting that grid-cell mechanisms could involve lower frequencies, but the low resonance strength in bat corresponds to smaller rebound depolarization that reduces the capacity to generate grid-cell periodicity in both oscillatory interference and attractor models (*28*).

Previous data indicate that I_h in rodent stellate cells is critical for theta-frequency sMPR (*8*, *24*). Our recordings from layer II neurons in bat mEC reveal a notable sag response and expression of

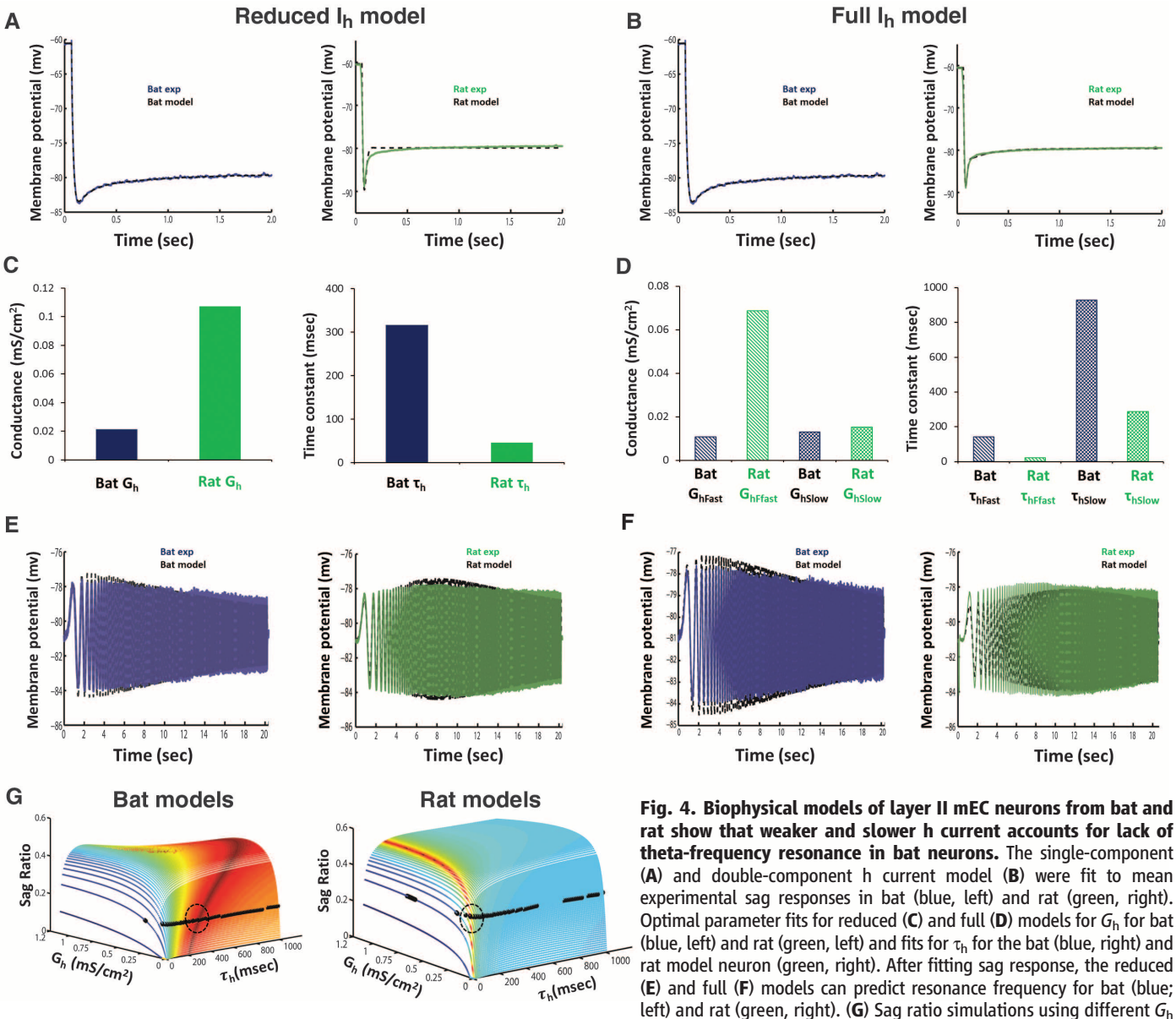

Fig. 4. Biophysical models of layer II mEC neurons from bat and rat show that weaker and slower h current accounts for lack of theta-frequency resonance in bat neurons. The single-component (**A**) and double-component h current model (**B**) were fit to mean experimental sag responses in bat (blue, left) and rat (green, right). Optimal parameter fits for reduced (**C**) and full (**D**) models for G_h for bat (blue, left) and rat (green, left) and fits for τ_h for the bat (blue, right) and rat model neuron (green, right). After fitting sag response, the reduced (**E**) and full (**F**) models can predict resonance frequency for bat (blue; left) and rat (green, right). (**G**) Sag ratio simulations using different G_h (1×10^{-6} to 1×10^{-4} S/cm^2) and activation time constants (5 to 1000 ms). Black circles show densities and time constants matching experimental sag ratio for bat (left) and rat (right). Color shows difference between model and experimental sag time constants for bat (left) and rat (right).

I_h. However, our simulations indicate that the non–theta-rhythmic response in the bat is due to smaller and slower h current than in rat stellate cells, similar to the smaller sag seen in nonhuman primates (*29*). Mice with forebrain-restricted HCN1 knockout (*30*) exhibit grid cells with larger size and spacing of grid fields compared with those of controls. Knockout of HCN1 reduced theta frequency sMPR (*8*, *24*), suggesting the increase in spacing resulted from decreased resonance frequency and supporting the hypothesis that resonance contributes to grid-cell formation in rodents. However, lack of theta rhythmic resonance in bat suggests an alternative interpretation that theta-frequency sMPR is not necessary for grid cells in the rodent. I_h underlies other neuronal properties, including control of resting membrane potential, spiking threshold, bistability, normalization of synaptic input, time course of after-hyperpolarization potentials, and synaptic integration and shape of synaptic responses (*24*, *26*, *31*–*35*). I_h could therefore influence grid-cell properties through mechanisms independent of theta-frequency resonance.

Rodentia and Microchiroptera are phylogenetically distant (*36*), and the absence of theta rhythmicity in bats (*5*, *17*) raises the question of whether grid cells could have arisen independently in the two lineages because of similar selective pressures for spatial navigation. Evidence for convergent neural coding across species can be found in sound localization and olfaction (*37*–*39*). Until evidence for convergent evolution in grid-cell formation is established, slice and whole-animal recordings from bats challenge models of space representation that rely on continuous theta rhythm.

References and Notes

1. M. Fyhn, S. Molden, M. P. Witter, E. I. Moser, M.-B. Moser, *Science* **305**, 1258 (2004).
2. T. Hafting, M. Fyhn, S. Molden, M.-B. Moser, E. I. Moser, *Nature* **436**, 801 (2005).
3. C. F. Doeller, C. Barry, N. Burgess, *Nature* **463**, 657 (2010).
4. N. J. Killian, M. J. Jutras, E. A. Buffalo, *Nature* **491**, 761 (2012).
5. M. M. Yartsev, M. P. Witter, N. Ulanovsky, *Nature* **479**, 103 (2011).
6. C. B. Canto, M. P. Witter, *Hippocampus* **22**, 1277 (2012).
7. L. M. Giocomo, E. A. Zilli, E. Fransén, M. E. Hasselmo, *Science* **315**, 1719 (2007).
8. L. M. Giocomo, M. E. Hasselmo, *J. Neurosci.* **29**, 7625 (2009).

9. A. Boehlen, U. Heinemann, I. Erchova, *J. Neurosci.* **30**, 4585 (2010).
10. J. G. Heys, L. M. Giocomo, M. E. Hasselmo, *J. Neurophysiol.* **104**, 258 (2010).
11. P. D. Dodson, H. Pastoll, M. F. Nolan, *J. Physiol.* **589**, 2993 (2011).
12. T. Hafting, M. Fyhn, T. Bonnevie, M. B. Moser, E. I. Moser, *Nature* **453**, 1248 (2008).
13. A. Jeewajee, C. Barry, J. O'Keefe, N. Burgess, *Hippocampus* **18**, 1175 (2008).
14. H. Stensola *et al.*, *Nature* **492**, 72 (2012).
15. M. P. Brandon *et al.*, *Science* **332**, 595 (2011).
16. J. Koenig, A. N. Linder, J. K. Leutgeb, S. Leutgeb, *Science* **332**, 592 (2011).
17. N. Ulanovsky, C. F. Moss, *Nat. Neurosci.* **10**, 224 (2007).
18. C. Barry, D. Bush, J. O'Keefe, N. Burgess, *Nature* **488**, E1, discussion E2 (2012).
19. E. H. Buhl, J. F. Dann, *Hippocampus* **1**, 131 (1991).
20. C. W. Gatome, L. Slomianka, D. K. Mwangi, H.-P. Lipp, I. Amrein, *Brain Struct. Funct.* **214**, 375 (2010).
21. A. Alonso, R. R. Llinás, *Nature* **342**, 175 (1989).
22. A. Alonso, R. J. Klink, *J. Neurophysiol.* **70**, 128 (1993).
23. C. T. Dickson *et al.*, *J. Neurophysiol.* **83**, 2562 (2000).
24. M. F. Nolan, J. T. Dudman, P. D. Dodson, B. Santoro, *J. Neurosci.* **27**, 12440 (2007).
25. J. S. Haas, A. D. Dorval 2nd, J. A. White, *J. Comput. Neurosci.* **22**, 161 (2007).
26. J. T. Dudman, M. F. Nolan, *PLOS Comput. Biol.* **5**, e1000290 (2009).
27. L. M. Giocomo, M.-B. Moser, E. I. Moser, *Neuron* **71**, 589 (2011).
28. Z. Navratilova, L. M. Giocomo, J. M. Fellous, M. E. Hasselmo, B. L. McNaughton, *Hippocampus* **22**, 772 (2012).
29. C. A. Buckmaster, H. Eichenbaum, D. G. Amaral, W. A. Suzuki, P. R. Rapp, *J. Neurosci.* **24**, 9811 (2004).
30. L. M. Giocomo *et al.*, *Cell* **147**, 1159 (2011).
31. D. L. F. Garden, P. D. Dodson, C. O'Donnell, M. D. White, M. F. Nolan, *Neuron* **60**, 875 (2008).
32. J. C. Magee, *Nat. Neurosci.* **2**, 848 (1999).
33. T. Berger, M. E. Larkum, H. R. Lüscher, *J. Neurophysiol.* **85**, 855 (2001).
34. S. R. Williams, S. R. Christensen, G. J. Stuart, M. Häusser, *J. Physiol.* **539**, 469 (2002).
35. N. A. Otmakhova, J. E. Lisman, *J. Neurophysiol.* **92**, 2027 (2004).
36. W. J. Murphy *et al.*, *Nature* **409**, 614 (2001).
37. L. M. Kay, M. Stopfer, *Semin. Cell Dev. Biol.* **17**, 433 (2006).
38. J. W. Schnupp, C. E. Carr, *Nat. Neurosci.* **12**, 692 (2009).
39. C. Y. Su, K. Menuz, J. R. Carlson, *Cell* **139**, 45 (2009).

Acknowledgments: We thank J. Ahn, J. Barcelo, C. Carr, W. Chapman, and M. Roesch for technical assistance and N. Spruston, J.-W. Lin, H. Eichenbaum, C. Stern, T. Gardner, and N. Ulanovsky for advice and comments. N. Ulanovsky and Y. Yovel helped us acquire Egyptian fruit bats for studies in supplementary materials. Research supported by Office of Naval Research grant N00014-12-1-0339 and Multidisciplinary University Research Initiative N00014-10-1-0936.

Supplementary Materials

www.sciencemag.org/cgi/content/full/340/6130/363/DC1
Materials and Methods
Supplementary Text
Figs. S1 to S3
References (*40*–*45*)

10 December 2012; accepted 27 February 2013
10.1126/science.1233831

Representation of Three-Dimensional Space in the Hippocampus of Flying Bats

Michael M. Yartsev and Nachum Ulanovsky*

Many animals, on air, water, or land, navigate in three-dimensional (3D) environments, yet it remains unclear how brain circuits encode the animal's 3D position. We recorded single neurons in freely flying bats, using a wireless neural-telemetry system, and studied how hippocampal place cells encode 3D volumetric space during flight. Individual place cells were active in confined 3D volumes, and in >90% of the neurons, all three axes were encoded with similar resolution. The 3D place fields from different neurons spanned different locations and collectively represented uniformly the available space in the room. Theta rhythmicity was absent in the firing patterns of 3D place cells. These results suggest that the bat hippocampus represents 3D volumetric space by a uniform and nearly isotropic rate code.

Navigation is crucial for survival, and the need to navigate cuts across the animal kingdom. Several navigational strategies are used by animals, among them maplike navigation (*1*). This strategy relies on a set of brain structures, at the hub of which is the hippocampus (*1*, *2*). This brain area contains "place cells," neurons that activate when the animal enters a restricted region of the environment, the place field (*1*, *2*). Since the discovery of place cells in rodents, these neurons have been reported across mammalian species (*1*–*9*), and their functional properties have been extensively researched (*1*, *2*). However, the spatial and temporal properties of place cells have never been studied in animals moving freely through 3D volumetric space, without any constraints to particular planes of motion. Indeed, in all studies to date, animals have always been navigating on one- or two-dimensional (2D) planes (*1*, *10*)—either horizontal (*5*, *7*, *11*–*15*), tilted (*3*, *4*, *16*–*18*), or vertical (*9*, *13*, *16*)—and thus it remains unresolved how place cells encode the animal's position throughout the entire volume of a 3D volumetric space. We developed wireless recording methodology for freely flying animals (*19*) and recorded single-neuron activity from hippocampal area CA1 of Egyptian fruit bats flying through 3D space.

Bats were tested in one of two setups: either a large cuboid-shaped flight room, where bats performed a naturalistic foraging task (Fig. 1A and fig. S1; room size 580 × 460 × 270 cm; n = 3 bats) or a 3D cubic flight arena of smaller dimensions, where bats searched randomly for food (fig. S2; room size 290 × 280 × 270 cm; n = 2 bats) (*19*). In both setups, bats exhibited complex naturalistic flight trajectories, during which they moved through all the three dimensions of the room (Fig. 1B and fig. S3), traversed large distances (Fig. 1C, left), and flew at high speeds (Fig. 1C, right; and fig. S4). These flight maneuvers resulted in dense and rather uniform coverage of the environment's 3D volume (figs. S5 and S6).

Single-unit activity was recorded from freely flying bats, using a tetrode-based microdrive and a custom lightweight four-channel neural telemetry system designed for flying bats (Fig. 1, D to F, and figs. S7 to S10). The telemetry system allowed the transmission of action potentials from the four channels of one tetrode, with high fidelity (Fig. 1, D, E, and G, and figs. S7 to S9), throughout all the locations in the flight room (figs. S7 and S8) and with very little interference from movement-related noise (fig. S11) (*20*).

The ability to monitor 3D spatial position and record the activity of individual neurons in freely flying bats allowed studying the spatial coding of 3D volumetric space by hippocampal neurons. We recorded a total of 139 well-isolated neurons from five bats in the dorsal CA1 region of the hippocampus (*19*). About half of the cells [73 out of 139 (73/139) or 53%] were active during flight, and 75% of the active cells (55/73) were classified as place cells (fig. S12), becoming active when the bat flew through a restricted volume of the available environment (*19*). Figure 2, A to E, shows the spatial spiking activity of a single hippocampal neuron recorded during flight. This neuron fired nearly exclusively in a confined region of the environment, and this region was restricted in all three dimensions (Fig. 2, A and B, and fig. S13). The firing field of this neuron remained highly stable across the recording session, both in its spatial location and its firing rate (Fig. 2, C and D, and fig. S14A); furthermore, the cell was reliably activated on most of the individual flight passes through the place field (Fig. 2E). Likewise, the majority (75%) of neurons that were active during flight

Department of Neurobiology, Weizmann Institute of Science, Rehovot 76100, Israel.

*Corresponding author. E-mail: nachum.ulanovsky@weizmann.ac.il